

Ride Comfort Optimization via Speed Planning and Preview Semi-Active Suspension Control for Autonomous Vehicles on Uneven Roads

处理路面预瞄信息；
可变时域MPC控

Hongliang Zhou, Zhiyuan Liu, *Member, IEEE*, and Mingqin Gu

Abstract—By simultaneously utilizing preview and global road information, a comfort optimization strategy which combines vehicle speed planning and preview semi-active suspension control is designed for autonomous vehicles. Considering that the impact of vehicle speed at the suspension vibration source is always a barrier for preview suspension control, a processing method for the road data is novelly proposed. Then, to utilize the processed data and to handle the nonlinearity of semi-active actuators, a hybrid horizon-varying (HV) model predictive control (MPC) method is given. The method can adapt to speed variation and meanwhile take the most of the road data within a fixed preview length. Further, based on the global information and considering multiple road irregularities in a driving path, a speed planning problem is established in the spatial domain and a dynamic programming based solution is provided. The final speed trajectory can compromise the driving time, vertical vibration and longitudinal acceleration. Various simulation results have been employed to verify the superiority of the hybrid HV-MPC method and the significance of speed and suspension coordination for comfort improvement.

Index Terms—autonomous vehicles, speed planning, semi-active suspension, preview control.

I. INTRODUCTION

THE development of sensing and control technology is rapidly pushing the automotive industry into the fields of intelligence and autonomy, and it has brought many new ideas and challenges about technology innovation [1] [2] [3]. Presently, research works on autonomous vehicles are mainly concentrated in environmental perception [4] [5] and trajectory planning [6] [7]. Based on these technologies, many safety solutions under complex traffic conditions have been obtained. However, almost all of these solutions were carried out on a smooth road surface, and the comfort issue under uneven road is rarely involved for autonomous vehicles. Additionally, for the comfort improvement of traditional vehicles, besides the shock absorption of suspension systems, experienced drivers will also adjust the vehicle speed according to the road condition and the comfort feeling. However, autonomous vehicles

Copyright (c) 2015 IEEE. Personal use of this material is permitted. However, permission to use this material for any other purposes must be obtained from the IEEE by sending a request to pubs-permissions@ieee.org.

This work is supported by China Automobile Industry Innovation and Development Joint Fund (No. U1564213) and National Natural Science Foundation of China (No. 61790562). (*Corresponding author: Zhiyuan Liu*)

J. Wu (email: vijaychn217@gmail.com), H. Zhou (email: zhouhongliang@hit.edu.cn) and Z. Liu (email: liuz_y@hit.edu.cn) are with the Department of Control Science and Engineering, Harbin Institute of Technology, Harbin 150080, China. M. Gu (email: mingqin.gmq@alibaba-inc.com) is with the Alibaba AI lab, Hangzhou 310000, China

lack subjective evaluation capabilities, and it will be difficult to automatically adjust the driving behavior according to the comfort requirement. Focus on this problem and based on the road information obtained from the network and the front view sensor, this paper is dedicated to finding a comfort control strategy that coordinates speed and suspension.

For traditional vehicles, suspension systems are key vehicle components to ensure the comfort performance. In order to break through the limits of traditional passive suspensions, active and semi-active suspensions have been researched for decades. Further, considering the high cost, complex structure and great energy consumption of active suspensions [8] [9] [10], semi-active suspensions, which employs an adjustable damper (magneto-rheological [11], electro-rheological [12], etc.) and has the advantages of easy installation, compact mechanism, quick response and extremely low energy consumption, are promising alternatives. Up to now, a number of semi-active control methods have been developed. For example, Skyhook and Acceleration-Driven-Damper [13], which suppress sprung mass vibration, and the Groundhook [14], which mitigates unsprung mass vibration, are classical methods. Subsequently, to balance comfort and handling, LQG (linear quadratic Gaussian) [15] and H_∞ [16] theories are applied with a clipped strategy. However, researchers claim in [17] that the clipped strategy which ignores the actuator capability would lead to performance deterioration, and a hybrid MPC (model predictive control) method is proposed for the actuator saturation. Further, fast calculations are realized with explicit MPC and neural network in [18] and [19], respectively. In addition, novel constrained H_∞ methods based on LPV (linear parameter varying) and PWA (piecewise affine) modeling can also be found in [20] and [21], respectively. Therefore, processing constraint is a necessary condition of semi-active controller design.

With the development of sensor technology, the information of oncoming road elevation (preview) is applied to the control system design for suspension performance enhancement. Specifically, it is found in [22] that the performance of semi-active suspension can be effectively improved with preview once the hard constraints are satisfied. In [23], the preview semi-active suspension is stated to be useful in two ways: 1) countering the adverse influences of actuation delays; 2) improve the control strategy directly over non-preview systems. Additionally, it is found that the major benefits are derived from the first 0.1s preview. In [24], a preview H_∞ controller is designed for a magneto-rheological (MR) suspension, and

in-depth analysis shows that the system can approach the performance of a non-preview active suspension. Recently, due to the constraint handling capability, MPC-based preview control has received much attention [25] [26]. In [26], by utilizing road information for the front 2s, it is confirmed that preview mechanism can improve the transient performance of semi-active suspensions. The above methods all require the road information within a fixed time. In practice, however, the road measurement is always performed with a fixed distance. Thus, the above methods are only applicable to constant vehicle speed conditions. Additionally, as concluded in [23], high speed may call for an extremely long preview distance once the preview time is fixed. To solve these problems, a speed-dependent preview controller has been recently given in [27], but only the random road described by filtered white noise can be handled. Actually, some innovative estimation methods for random roads have also been given for time-varying condition [28]. However, design the preview controller under a variable speed for general road profile is still an urgent problem.

For autonomous vehicles, not only the road information ahead is available, but also the road undulation of the entire driving path can be grasped through the rapidly developing IoT (Internet of Things) system. As evidence, in [29], the transmission of the risk index of each road segment has been realized through the V2C2V (vehicle-to-cloud-to-vehicle) network for safety-based path planning. Similarly, in [30], the elevation estimation result of each road segment is uploaded to the V2C2V network, and a comfort-based path is planned. In addition, a large number of solutions for road height estimation [31] [32] and network latency [33] [34] [35] have been provided. The road information of the entire path is absolutely unnecessary for the high-bandwidth suspension system. However, the information can be used for vehicle speed planning to indirectly influence the vertical vibration, since road surface and vehicle speed are the two factors that determine the vibration source [36]. Then, an interesting question arises as that: *Is it possible to achieve better comfort performance through speed planning?* Since the vibration will disappear when the speed is zero, a precondition for this question is that a sufficient speed should be ensured for the longitudinal passing ability. Clearly, if the relationship between speed and comfort performance is non-monotonic, the question will lead to a multi-objective planning problem. However, to the best of our knowledge, current speed planning issues are mostly limited to traffic efficiency, safety, and energy consumption [37] [38], and rare research has been focused on the comfort issue.

The above description gives three main research stages that vehicle comfort goes through as information becomes more abundant, and each stage has specific issues that need to be addressed, for example, 1) the nonlinear actuator characteristics in traditional suspension control, 2) the speed-adaptive capability in preview suspension control, and 3) speed planning problem in unmanned vehicles. Focusing on the above issues, and considering that existing speed planning researches are mainly focused on safety and fuel economy issues, this article attempts to coordinate the vertical movement (suspension) and the longitudinal movement (vehicle speed) from

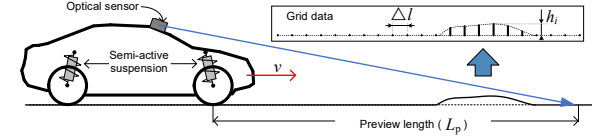


Fig. 1. Semi-active suspension with road preview.

the perspective of vehicle comfort. An expected application mechanism is that: the semi-active suspension uses finite road information for vertical control, while the transmission system uses the global road information for vehicle speed adjustment. To realize this mechanism, the following contributions are made in this paper:

- By defining road profile information (including preview and global information) and vertical dynamics and constraints of semi-active suspension, a multi-objective problem which involves suspension control and speed planning is proposed;
- To make full use of the preview information, a road information processing method is given. The method can transform spatial-domain data into different time-domain data according to different vehicle speeds. Furthermore, the obtained data can effectively reflect the influence of vehicle speed on the vibration frequency;
- To handle the actuator constraints of suspension, a hybrid logic MPC method is adopted. Further, to utilize and adapt to the speed-dependent time-domain preview data, a horizon-varying mechanism is creatively proposed, which finally leads to a hybrid horizon-varying MPC (HV-MPC) suspension controller;
- With the global road information, we establish a speed planning problem in the spatial domain. The final speed trajectory is obtained by optimizing the vibration, the driving time and the vehicle acceleration (deceleration) simultaneously with the employment of the dynamic programming (DP) principle;
- Since the preview suspension control is designed to be speed adaptive and will not influence the speed planning, the vertical and longitudinal systems can work in harmony for the comfort enhancement. Finally, the significance of the coordinated operation is verified at different speeds and road profiles.

The remainder of this paper is organized as follows. Section II introduces the semi-active suspension dynamics, the road information, and the multi-objective problem. Furthermore, in Section III, we introduce the information processing method and the design of the hybrid HV-MPC controller. In Section IV, the speed planning problem is formulated together with the DP solution. The simulation analysis is given in Section V and the conclusions are drawn in Section VI.

II. PROBLEM FORMULATION

A. Road Profile Information

Due to the strong environmental perception ability of autonomous vehicles, two kinds of road profile information are considered in this paper: 1) the preview road information

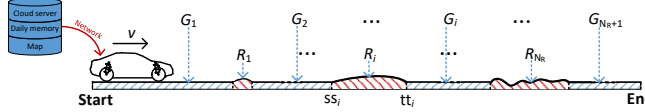


Fig. 2. Schematic of global road information.

shown in Fig. 1, and 2) the global road information of a specific driving path shown in Fig. 2. The preview information is obtained from a vehicle-mounted optical sensor, which leads to a high positional accuracy but short preview length. Inversely, the global road information can be obtained from the V2C2V network, the memory of daily road or the future high precision map. This information can provide a long road view, but the positional accuracy is limited by GPS systems. Specific features of the two information will be described below.

In Fig. 1, L_p is a constant preview length and v denotes the real-time speed. Applying proper signal processing method, the influence of body attitude on road measurement can be eliminated [32], which results in the grid data shown in Fig. 1. For convenience, we consider that the grid points are evenly distributed in space with a constant interval Δl . Actually, the magnitude of Δl is highly related to the capability of optical sensors and is considered to be sufficient precise in this paper. Therefore, the preview information can be expressed with a set $\Omega(t)$ as that:

$$\Omega(t) = \{h_1(t), h_2(t), \dots, h_{N_{sp}}(t)\} \quad (1)$$

where $h_i(t)$ indicates the road height of the i -th grid point at time t , N_{sp} is the grid number which satisfies that

$$N_{sp} = \lfloor \frac{L_p}{\Delta l} + 1 \rfloor. \quad (2)$$

Obviously, $\Omega(t)$ is defined in the spatial domain, which cannot be directly used by the time-domain defined dynamic system. Traditional preview suspension control methods always solve this problem by simply setting that $t_p = L_p/v$, where t_p is a constant preview time shown in Fig. 3. However, this solution is only applicable when v is constant. Therefore, a method to properly utilize $\Omega(t)$ under a time-varying speed should be designed.

In Fig. 2, the entire road is divided into two kinds of road segments: rough road R_i , $i = \{1, \dots, N_R\}$ and general road G_i , $i = \{1, \dots, N_R + 1\}$. The segment R_i represents the profile with large fluctuations, for example, speed bumps, potholes, long-wave fluctuations caused by long-term vehicle rolling or crustal movement, etc.. Conversely, G_i denotes the segment with relatively small fluctuations, such as normal asphalt roads, macadam road, stone road, etc.. In this paper, we specify that the characteristic parameters of R_i and G_i can be obtained as follows:

$$R_i = \{\text{ss}_i, \text{tt}_i, v_i^{\max}, v_i^{\min}, f_i\}, i = \{1, \dots, N_R\}, \quad (3a)$$

$$G_i = \{v_i^{\max}, v_i^{\min}\}, i = \{1, \dots, N_R + 1\}. \quad (3b)$$

where ss_i and tt_i are the start and terminal positions (including latitude and longitude) of R_i , respectively; v_i^{\max} and v_i^{\min} are the allowable maximum and minimum speeds of each segment, respectively; f_i is a function unique to R_i , which

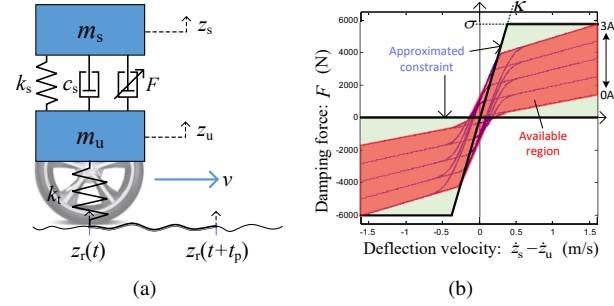


Fig. 3. (a) Quarter of vehicle model; (b) damping force constraint.

characterizes the relationship between road length and height. The division and definition of G_i and R_i is very necessary, since that: 1) R_i is more rigorous for comfort performance; 2) the profile of R_i is more easily to be identified by road estimators and described with a deterministic function [39], while that of G_i is generally a random profile. Presently, for the two types of roads G_i and R_i , we can only make qualitative distinctions from 1) the magnitude of road height and 2) the functional description of road surface. Other quantitative descriptions may be given in future studies, and is beyond the scope of this paper.

In this paper, we believe that the vertical vibration caused by G_i can be totally handled by suspension systems. However, for R_i , proper adjustment of speed v is necessary to improve the ride performance. What's more? Since the speed is time-varying, and the suspension control is always enabled for both G_i and R_i roads, a speed adaptive preview suspension controller should be designed firstly.

Remark 1: It should be noted that the preview road information and the global road information cannot replace each other. Firstly, the length L_p of the preview information is usually short. Therefore, using preview information to guide the speed control may cause dramatic speed variation. Secondly, the positioning errors from global information has little effect on the speed adjustment, but is unacceptable for the fast suspension control. Therefore, the global information will only be used for speed planning, and the preview information is only employed by suspension control.

Remark 2: The parameter v_i^{\max} can be obtained according to not only traffic laws, but also the safety-oriented speed planning results from traffic environment. Thus, the driving safety will always be the premise of comfort-oriented speed planning. In the event of unpredictable emergencies, the setting of v_i^{\max} will become irrelevant, since the comfort speed plan given in this paper can be turned off directly.

Remark 3: Parameter v_i^{\min} can also be obtained based on traffic laws. Without special safety regulations, v_i^{\min} can also be set as an arbitrarily small value or even zero. Since the comfort is definitely the best when the speed is zero, the driving time and comfort of the vehicle will be considered simultaneously in the speed planning process of the paper.

B. Dynamics of Semi-Active Suspensions

To design the preview suspension controller, a quarter of vehicle (QoV) model is shown in Fig. 3(a), where m_s is the sprung mass which represented the vehicle body; m_u is the unsprung mass, indicating the integrated mass of the hub, tire, shock absorber, spring and linkages; k_s is the spring stiffness; c_s is the coefficient of an additional passive damper; F is the output damping force of an adjustable damper; k_t is the equivalent stiffness of the tire; z_s and z_u represented the vertical displacement of the sprung and unsprung masses, respectively; z_r is the road height and v is the vehicle longitudinal speed. Based on these definitions, the dynamics of a semi-active suspension can be obtained according to Newton's law.

Specifically, choose state variables as follows:

$$\begin{aligned} x_1(t) &= z_s(t), & x_2(t) &= \dot{z}_s(t), \\ x_3(t) &= z_u(t), & x_4(t) &= \dot{z}_u(t), \end{aligned} \quad (4)$$

and control and disturbance inputs as that $u(t) = F(t)$ and $w(t) = z_r(t)$, respectively. Then, by defining

$$x(t) = [x_1(t) \ x_2(t) \ x_3(t) \ x_4(t)]^T, \quad (5)$$

the state-space expression can be obtained as that

$$\dot{x}(t) = \bar{A}x(t) + \bar{B}u(t) + \bar{B}_d w(t) \quad (6)$$

where

$$\begin{aligned} \bar{A} &= \begin{bmatrix} 0 & 1 & 0 & 0 \\ -\frac{k_s}{m_s} & -\frac{c_s}{m_s} & \frac{k_s}{m_s} & \frac{c_s}{m_s} \\ 0 & 0 & 0 & 1 \\ \frac{k_s}{m_u} & \frac{c_s}{m_u} & -\frac{k_s}{m_u} - \frac{k_t}{m_u} & -\frac{c_s}{m_u} \end{bmatrix}, \\ \bar{B} &= [0 \ -1 \ 0 \ 0]^T, \quad \bar{B}_d = [0 \ 0 \ 0 \ \frac{k_t}{m_u}]^T. \end{aligned}$$

As semi-active suspensions can only dissipate energy, Fig. 3(b) shows the available region of u according to the V/F (velocity/force) property of a MR damper. According to [21], this actuator shows different damping characteristics under different current values, and Fig. 3(b) shows the available damping force when the current varies between 0A to 3A. Further, applying the approximation method given in [17], the damping force constraint can be expressed as follows:

$$(x_2 - x_4)u \geq 0, \quad (7a)$$

$$|u| \leq \sigma, \quad (7b)$$

$$u(x_2 - x_4) \leq \kappa(x_2 - x_4)^2 \quad (7c)$$

where σ and κ are constants which denote the maximum force and the maximum dissipation power, respectively.

Remark 4: Although the description of this damping force constraint has some approximate errors, it can significantly reduce the complexity of system description. In addition, due to space limitations, this article does not consider the conversion of damping force to current during actual application, which involves the inverse model of certain type of actuators. Related research can refer to references [21] and [40].

C. Multi-Objective Problem

The speed planning of autonomous vehicles is always carried out under the constraints of safety and traffic law. However, the comfort problem resulted from uneven road is rarely considered. Generally, reducing vehicle speed is beneficial to improve the comfort performance, but will also leads to a decrease in maneuverability. Therefore, under the speed constraints, the goal of this paper is to improve the comfort and maneuverable performance by coordinating the speed and suspension. Obviously, this is a multi-objective optimization problem with the following requirements:

Q1: the driving time is minimized;

Q2: the comfort performance in each R_i is optimal;

Q3: the sum of $|\dot{v}|$ during the entire trip is minimized;

Q4: the preview suspension can adapt to the speed variation.

III. MPC-BASED PREVIEW SUSPENSION CONTROL

To understand and describe the effect of vehicle speed on vertical vibration, this section will firstly give a preview semi-active suspension control method for problem Q4. The resulting controller consists of two parts, namely, preview information processing module and hybrid VH-MPC module.

A. Preview Information Processing

In the following, the data set $\Omega(t)$ will be converted into a signal that can be utilized by the suspension control system based on the vehicle speed v .

Firstly, by assigning the sample period of suspension control system as T_s , the driving distance within each sample time can be obtained as that $l_s = vT_s$. Since the high precision of optical sensors and the road-scanning frequency can be independent of T_s , we consider that $\Delta l \ll l_s$. Based on this, the grid number that a vehicle pass through within kT_s can be obtained as

$$n(k, v) = \lfloor \frac{kl_s}{\Delta l} \rfloor = \lfloor \frac{kvT_s}{\Delta l} \rfloor. \quad (8)$$

Further, we assume that the road height between $h_i(t)$ and $h_{i+1}(t)$ satisfy zero-order retention and is equal to $h_i(t)$. Then, if the road height at time kT_s is h_i , the vehicle will reach the height of $h_{i+n(1,v)+1}$ when the time is $(k+1)T_s$. Thus, none of the grid data $h_{i+1}, h_{i+2}, \dots, h_{i+n(1,v)}$ can be utilized by the suspension control system. Based on this, we can obtain the set of available road height data Θ when the speed is v at time kT_s as follows:

$$\Theta(v, k) = \{H_1(v, k), H_2(v, k), \dots, H_{N_{tp}(v)}(v, k)\} \quad (9)$$

where

$$H_i(v, k) = h_{n(i-1,v)+1}(kT_s), i = 1, 2, \dots, N_{tp}(v), \quad (10a)$$

$$N_{tp}(v) = \lfloor \frac{(N_{sp}-1)\Delta l}{vT_s} \rfloor = \lfloor \frac{L_p}{vT_s} \rfloor. \quad (10b)$$

Here, $N_{tp}T_s$ is definitely t_p of traditional preview controllers and the difference is that the preview time here is speed dependent.

To vividly illustrate the above data processing, Fig. 4 shows the available preview data for a road segment when v is equal to $v_0, 2v_0$ and $3v_0$, respectively. According to Fig. 4, from

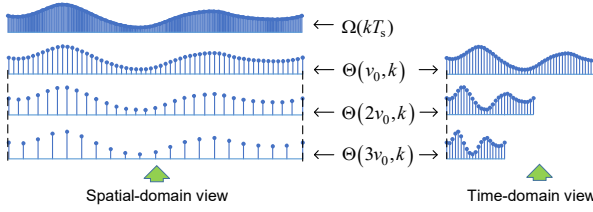


Fig. 4. Preview data under different vehicle speeds

the perspective of spatial domain, the change in v results in a change in the density of data points within L_p . This is because that $n(1, v)$ results in different data utilizations and different values of N_{tp} . While from the perspective of time domain, the change in v leads to the change in excitation frequency. This is because that the time interval of the processed data is always T_s . In summary, the given data processing method can objectively reflect the influence of v on the outer excitation of suspension systems.

B. Hybrid VH-MPC Based Preview Suspension Control

According to the above information processing results, to reflect the frequency-varying character of excitations caused by speed changes, it is necessary to make full use of the information $\Theta(v, k)$ with a time-varying amount N_{tp} . However, existing preview control methods can only use fixed-length data, for example the H_∞ preview control in [24] and the MPC based preview control in [25]. Therefore, to improve the suspension performance by totally using preview data $\Theta(v, k)$, this subsection will propose a novel preview controller to adapt the speed-dependent N_{tp} .

Define the suspension performance output vector as follows:

$$y(t) = [y_1(t) \quad y_2(t) \quad y_3(t)]^T \quad (11)$$

where $y_1 = \ddot{z}_s$ indicates the comfort performance, $y_2 = z_s - z_u$ represents the dynamic deflection of suspension and $y_3 = z_u - z_r$ represents the handling performance. Then, according to (4)-(6) and the sample time T_s , a discrete-time system equation can be obtained as follows:

$$x(k+1) = Ax(k) + Bu(k) + B_d w(k), \quad (12a)$$

$$y(k) = Cx(k) + Du(k) + D_d w(k) \quad (12b)$$

where A, B, C, D, B_d and D_d are discrete system matrices.

To handle the nonlinear state-dependent control constraint in (7), a hybrid logic modeling method in [17] is employed. Firstly, two Boolean variables δ_v and δ_F are defined as follows:

$$[\delta_v = 1] \leftrightarrow [x_2 - x_4 \geq 0], \quad [\delta_F = 1] \leftrightarrow [u \geq 0]. \quad (13)$$

Then, constraint (7a) equals to the following relationship:

$$[\delta_v = 1] \rightarrow [\delta_F = 1], \text{ and } [\delta_v = 0] \rightarrow [\delta_F = 0]. \quad (14)$$

Further, by defining an auxiliary variable z as that:

$$z = \delta_v(u - \kappa(x_2 - x_4)), \quad (15)$$

constraint (7c) can be expressed as:

$$u - \kappa(x_2 - x_4) - 2z \geq 0. \quad (16)$$

Finally, by defining $\delta = [\delta_v \quad \delta_F]^T$ and according to the modeling theory in [41], (7b) and (13)-(16) can be expressed as the following linear constraints:

$$\begin{cases} E_1\delta(k) + E_2z(k) \leq E_3u(k) + E_4x(k) + E_5, \\ E_6\delta(k) = 0 \end{cases} \quad (17)$$

where $E_i, i = \{1, \dots, 6\}$ are constant matrices. Thus, the nonlinear constraints have been expressed as linear hybrid logic constraints.

Based on the above discrete-time system and constraints, a moving horizon optimization can be established with model prediction. Firstly, for convenience, we assume that the prediction horizon N_p is equal to the control horizon N_c . Further, to use the preview data $\Theta(v, k)$ for state prediction, we specify that $N_p = N_{tp}(v(k))$ for any time instant k . Accordingly, by specifying δ, z and u as the decision variable, a prediction equation can be obtained as follows:

$$X(k) = \Sigma_1 x(k) + \Sigma_2 U(k) + \Sigma_3 W(k) \quad (18)$$

where $\Sigma_1, \Sigma_2, \Sigma_3$ are prediction matrices, $x(k)$ is the current state vector and

$$\begin{aligned} x(k) &= [x_1(k) \quad x_2(k) \quad x_3(k) \quad x_4(k)]^T, \\ X(k) &= [x_{k|k}, \dots, x_{k+N_{tp}-1|k}]^T, \\ W(k) &= [w_k, \dots, w_{k+N_{tp}-1}]^T, \\ U(k) &= [u_k, \dots, u_{k+N_{tp}-1}, \\ &\quad \delta_k, \dots, \delta_{k+N_{tp}-1}, z_k, \dots, z_{k+N_{tp}-1}]^T. \end{aligned}$$

In equation (18), $x_{k+i|k}$ denotes the predicted state, and $x_{k|k} = x(k)$. To achieve preview control, the elements in $W(k)$ are considered equal to those in $\Theta(v, k)$. By defining positive definite matrices $Q = Q^T \succ 0$ and $R = R^T \succ 0$, the objective function can be written as follows:

$$\begin{aligned} J_{\text{sas}}(U(k), x(k), N_{tp}(v(k)), W(k)) \\ = \sum_{i=0}^{N_{tp}-1} (y_{k+i|k}^T Q y_{k+i|k} + u_{k+i|k}^T R u_{k+i|k}) \end{aligned} \quad (19)$$

Since $v(k)$ may be different from $v(k+1)$, which results in different N_{tp} , a VH-MPC strategy is adopted here. The specific steps are as follows:

- 1) read $x(k)$ and $v(k)$ at time k ;
- 2) calculate N_{tp} and $W(k)$;
- 3) solve the following mixed integer quadratic problem:

$$\begin{aligned} \min_U J_{\text{sas}}(U(k), x(k), N_{tp}(v(k)), W(k)) \\ \text{s.t. (17) for all predictive steps;} \end{aligned} \quad (20)$$

- 4) set the first element of the solution sequence U as the actual control action;
- 5) repeat the whole procedure at time $k+1$.

This strategy actually constitutes a state-feedback controller and should be applied together with a state estimator to obtain $x(k)$ in the first step. Related works on the design of this estimator can be referred in [18] and [19], which will not be given in this paper. Obviously, the above variable horizon strategy is realized by switching among multiple controllers, then two issues will influence the actual application: 1) the length of N_{tp} for any single controller; 2) the switching frequency of multiple controllers. The first issue can be analyzed through equation (10b), while for the second issue, we define Δv as

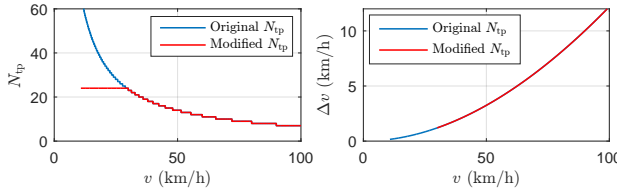


Fig. 5. Relationship between vehicle speed and controller switching.

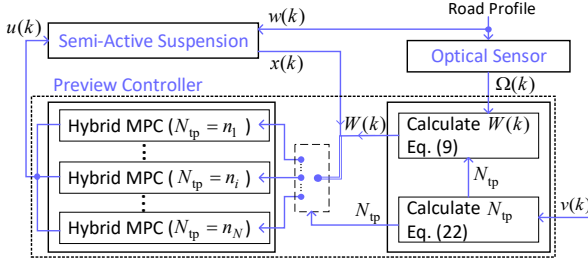


Fig. 6. Closed-loop system structure of the preview semi-active suspension.

the speed increment which may cause N_{tp} changes to $N_{tp} + 1$. Then, according to (10b), we can obtain that:

$$\Delta v = \frac{v^2 T_s}{L_p + v T_s}. \quad (21)$$

The blue lines in Fig. 5 depicts the changes of N_{tp} and Δv with v when $T_s = 5\text{ms}$ and $L_p = 1\text{m}$. According to Fig. 5, when v is reduced, N_{tp} will increase significantly and Δv will decrease to a small value. Thus, a small v will lead to heavy calculation burden of a single controller and make the switching of multiple controller sensitive. To this end, we modify the calculation of N_{tp} as follows:

$$N_{tp}(v) = \begin{cases} \left\lfloor \frac{L_p}{v^* T_s} \right\rfloor & \text{if } v \leq v^* \\ \left\lfloor \frac{L_p}{v T_s} \right\rfloor & \text{if } v > v^* \end{cases} \quad (22)$$

According to (22), when $v \leq v^*$, a fixed time preview control is used to reduce the computational difficulty and the switching sensitivity; when $v > v^*$, a fixed length preview control is realized to make the most of the information within the preview distance. The red lines in Fig. 5 show the modified results of N_{tp} and Δv when $v^* = 30\text{km/h}$ is specified in this paper.

Based on the above design process, Fig. 6 depicts the preview control structure for time-varying speed. It is worth noting that unlike the traditional VH-MPC strategies which need to calculate all pending controllers at the same time [42] [43], the proposed method only calculates one Hybrid MPC controller at a sample time. Thus, the computational efficiency can be significantly improved. Currently, rapid calculation of MPC is making great progress. In addition to the explicit MPC method in [18] and the neural network approximation method in [19], MPC applications based on FPGA platforms have also shown outstanding time efficiency in [44] and [45]. These techniques can further improve the practicability of the VH-MPC algorithm in this paper.

IV. VEHICLE SPEED PLANNING

For the vehicle's travel path which contains multiple independent rough roads R_i , this section will propose a method to achieve the optimal speed trajectory based on dynamic programming principle. Firstly, some basic assumptions are given as follows:

- 1) the speed remains constant when driving on rough roads R_i ;
- 2) the vertical vibration on general roads G_i can be ignored when we plan the speed;
- 3) the speeds at the start and end points are both zero.

Further, by defining L_f as the total distance of the driving path and L as the real-time distance, the optimal problems Q1-Q3 can be formulated in the spatial domain with the following cost function:

$$J_L(v) = \int_0^{L_f} \rho_1 \dot{J}_{ver}(v) + \rho_2 \dot{J}_{lon}(v) + \rho_3 \dot{J}_t(v) dL \quad (23)$$

where $\dot{J}_{ver}(v)$ denotes the vertical performance which is evaluated by a root-mean-square (RMS) value when the vehicle travels a unit distance dL with speed v ; Similarly, \dot{J}_{lon} is the longitudinal acceleration and \dot{J}_t is the travel time. Since obtaining explicit expressions for $\dot{J}_{ver}(v)$, \dot{J}_{lon} and \dot{J}_t is a nontrivial task, the following paper will propose a simulator to quantized the RMS-based vertical performance under rough roads and manipulate the global information to establish a solvable planning problem.

A. Vertical Performance Simulator

A simulator is proposed here to calculate the vertical performance when the vehicle pass through a rough road R_i (road length \bar{l} and height function \bar{f}) with a speed v . The simulation time interval is set as T_{sim} . The RMS quantized vertical performance \bar{C} are described by the following function:

$$\bar{C}(v, \bar{l}, \bar{f}) = \frac{v}{\bar{l}} \int_0^{\frac{\bar{l}}{v}} \tau_1 y_1^2(t) + \tau_2 y_2^2(t) + \tau_3 y_3^2(t) dt \quad (24)$$

where τ_1 , τ_2 and τ_3 are weighting coefficients and the weights are the same with Q in (19). Firstly, we get the suspension excitation by using the data processing method in section III-A. This can be realized by setting $L_p = \bar{l}$, and then use Δl and \bar{f} to obtain a spatial data set Ω . Then, a time-domain excitation set Θ can be acquired by using (9) and (10) with that $T_s = T_{sim}$. It should be noted that T_{sim} is used only for excitation generation. Once a small T_{sim} is chosen, the excitation data under different speeds can be more clearly obtained with a big data set. However, a small T_{sim} will not obviously increase the calculation complexity, since the simulator is only activated at every sample time T_s . By driving a QoV model with Θ , \bar{C} can be obtained with (24). Two issues should be noted for this simulator: 1) when calculate Θ , the data number N_{tp} satisfies (10b) instead of (22). This is because that (22) cannot simulate the excitation at low speed; 2) A passive suspension with that $F = c_s^*(\dot{z}_s - \dot{z}_u)$ and $c_s^* = 3000\text{Ns/m}$ is used in the QoV model to avoid excessive calculations. The calculated \bar{C} will be used in the following speed planning problem.

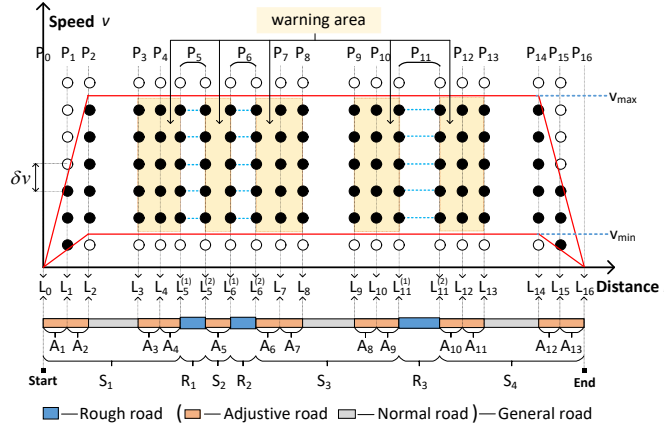


Fig. 7. Schematic diagram of global information manipulation

B. Manipulation of Global Information

The global information will be manipulated in this subsection to establish a dynamic programming problem. To facilitate the description, Fig. 7 gives the manipulation diagram where 3 rough roads and 4 general roads are encountered. Specific manipulation steps are described as follows:

Step1: Since the speed adjustment sections are mainly located around the start point, the end point and the rough roads, we divide the related G_i roads into adjustive roads and normal roads. To make the wide range of speed changes in adjustive road possible, the length of each adjustive road is specified as that $l_{a1} = 200m$. Further, to detail the speed trajectory within each adjustive road, we divide l_{a1} into 4 subsegments with an interval $l_{a2} = 50m$. In Fig. 7, only 2 subsegments for each adjustive road are depicted due to the space limitation and $A_i, i = \{1, \dots, 13\}$ are subsegments. For the case where the distance between adjacent R_i roads is less than $2l_{a1}$, such as R_1 and R_2 in Fig. 7, the middle general road is considered as an complete adjustive road and is further divided into subsegments properly.

Step2: By specifying that the speed in each A_i changes linearly, the speed planning problem becomes the designation of the initial and terminal speeds for all A_i . Based on this, all of the points waiting for speed specification, for example $P_i, i = \{0, \dots, 16\}$ in Fig. 7, can be obtained. Since the speed in R_i road is constant, P_i may be a rough road in addition to a location point.

Step3: Set each P_i with characteristic parameters as that

$$P_i = \{L_i^{(1)}, L_i^{(2)}, v_i^{\max}, v_i^{\min}, G_i\}. \quad (25)$$

In (25), $L_i^{(1)}$ and $L_i^{(2)}$ denote the distance from ss_i and tt_i to the start point, respectively, when P_i indicates rough road R_i . Otherwise, if P_i is a location point, then $L_i^{(1)} = L_i^{(2)} = L_i$. Further, v_i^{\max} and v_i^{\min} denote the allowable speed range of P_i , which can be directly obtained from (3). The parameter G_i is a data set as follows:

$$G_i = \{\bar{C}_i(v_1), \bar{C}_i(v_2), \dots, \bar{C}_i(v_M)\} \quad (26)$$

where $\bar{C}_i(v_j), j = \{1, \dots, M\}$ denotes the vertical performance when the vehicle pass P_i with a speed v_j , and the

size of M relates to a chosen speed interval δv . In this paper, we set that $\delta v = 3.6km/h$. Obviously, \bar{C}_{ij} can be obtained by run the pre-designed simulator when P_i indicates R_i , and $\bar{C}_{ij} = 0$ if P_i is a point. However, for the points near a rough road (the warning areas in Fig. 7), we artificially set a nonzero vertical performance. Specifically, if P_i is a rough road, then for the points $P_{i-3}, P_{i-2}, P_{i-1}, P_{i+1}, P_{i+2}$ and P_{i+3} , we set that:

$$\begin{aligned} \bar{C}_{i-1,j} &= \bar{C}_{i+1,j} = 0.75\bar{C}_{i,j}, \\ \bar{C}_{i-2,j} &= \bar{C}_{i+2,j} = 0.5\bar{C}_{i,j}, \\ \bar{C}_{i-3,j} &= \bar{C}_{i+3,j} = 0.25\bar{C}_{i,j}. \end{aligned} \quad (27)$$

This evenly increment (or decrement) of \bar{C}_{ij} is very important, since it warns the vehicle that a rough road is coming (or staying away). For adjacent R_m and R_{m+1} with short distances, this evenly distribution can also be realized between $\bar{C}_{m,j}$ and $\bar{C}_{m+1,j}$.

C. Dynamic Programming

According to DP principle, the globally optimal speed trajectory can be proceeds backward from P_N to P_0 by solving the following minimization problem:

$$J_i(v_i) = \min_{v_i \in \mathcal{V}_i} \{g_i(v_i) + J_{i+1}(v_{i+1})\}, i = \{1, \dots, N\} \quad (28)$$

where $J_i(v_i)$ is the cost-to-go function from point i to N starting from v_i with terminal cost $J_N(v_N) = g_N(V_N)$; $\mathcal{V}_i = [v_i^{\min}, v_i^{\max}]$ defines the speed range. Since the terminal speed is limited to zero, we define $g_N(v_N) = 0$ when $v_N = 0$, otherwise $g_N(v_N) = \infty$. According to (24), the transition cost function from point i to $i+1$ for $i = 0, 1, \dots, N-1$ is defined as:

$$g_i(v_i) = \begin{cases} \psi(v_i) & \text{if } v_i \in \mathcal{V}_i \\ \infty & \text{otherwise} \end{cases} \quad (29)$$

where

$$\begin{aligned} \psi(v_i) &= \rho_1 \bar{C}_i(v_i) + \rho_2 \left| \frac{v_i^2 - v_{i+1}^2}{L_i^{(2)} - L_{i+1}^{(1)}} \right| \\ &\quad + \rho_3 \left(\frac{L_i^{(2)} - L_i^{(1)}}{v_i} + \left| \frac{2(L_{i+1}^{(1)} - L_i^{(2)})}{v_{i+1} - v_i} \right| \right). \end{aligned} \quad (30)$$

In expression (30), $\bar{C}_i(v_i)$ is the vertical performance of P_i , $\left| \frac{v_i^2 - v_{i+1}^2}{L_i^{(2)} - L_{i+1}^{(1)}} \right|$ denotes the longitudinal acceleration from P_i to P_{i+1} , and $\frac{L_i^{(2)} - L_i^{(1)}}{v_i} + \left| \frac{2(L_{i+1}^{(1)} - L_i^{(2)})}{v_{i+1} - v_i} \right|$ is the driving time. Specifically, $\frac{L_i^{(2)} - L_i^{(1)}}{v_i}$ is the time when the vehicle pass through P_i (the time is zero once P_i is a position point) and $\left| \frac{2(L_{i+1}^{(1)} - L_i^{(2)})}{v_{i+1} - v_i} \right|$ is the time when the vehicle runs from P_i to P_{i+1} .

Accordingly, the optimal speed trajectory $V^* = \{v_0^*, v_1^*, \dots, v_N^*\}$ can be obtained by searching the speed with the interval δv such that J_i from N to 0 is minimized and $v_0^* = 0$.

Fig. 8 shows how the planning result V^* affects the longitudinal and vertical dynamics. Specifically, V^* will firstly be given to the powertrain control system to realize the speed tracking. Then, the actual real-time speed $v(k)$ will

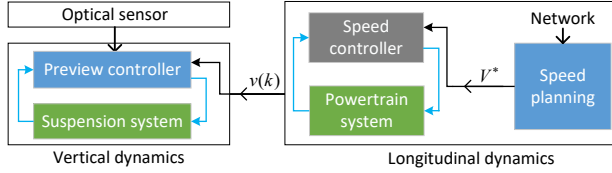


Fig. 8. Overall system structure and relationship between subsystems

TABLE I
PARAMETERS OF THE QOV MODEL

m_s	m_u	k_s	k_t	c_s	κ	σ
450kg	75kg	27kN/m	200kN/m	2kNs/m	7kNs/m	6.5kN

further influence the switching of the Hybrid HV-MPC based suspension controller.

Remark 5: The vertical and longitudinal control systems can run in harmony. An important issue for the effective operation is that: only the longitudinal dynamics with a low bandwidth can affect the vertical dynamics with a relatively high bandwidth. The vertical suspension controller is always enabled for arbitrary road segments and can adapt but not influence the speed adjustment. As a modification of the speed planning, a full vehicle model can also be used in the vertical performance simulator to evaluate the roll and pitch motions. But in this paper, only the vertical vibration is considered, so the concise QoV model is employed.

Remark 6: The speed controller and the powertrain system is omitted in this paper, thus the planned speed is assumed to be realized without deviation.

Remark 7: For roads with a very low proportion of rough roads, the global road information here can also be used to describe local roads that contain rough segments. In this condition, the boundary speeds v_0 and v_N can be set to non-zero states for the given planning method.

V. SIMULATION AND ANALYSIS

In this section, the hybrid HV-MPC method will be applied to a quarter of car model described in Section II. The model parameters are listed in Table I, where the constraint parameters κ and σ are obtained according to the test data of a prototype MR damper from the FAW-Tokico Corporation [11]. Then, the control performance will be analyzed under different road and speed conditions. In the end, we combine the proposed controller with the speed planning method and apply it to a path with multiple road conditions for multi-objective performance evaluation.

A. Comfort Performance at Constant Speed

The performance of the hybrid HV-MPC method at various constant speeds and typical roads will be simulated here. In addition, to more clearly reflect the characteristics of the proposed controller, we simultaneously evaluate the suspension performance with a sample time $T_s = 5\text{ms}$ and a simulation step of 1ms for the following control methods. The T_{sim} which

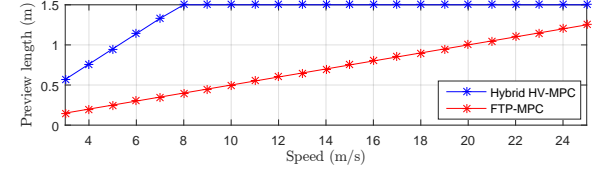


Fig. 9. Preview length of Hybrid HV-MPC and FTP-MPC methods at different speeds.

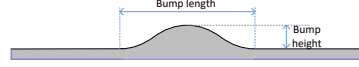


Fig. 10. A independent bump road.

is used for excitation generation under different speed is also set as 1ms.

Hybrid HV-MPC: The preview controller proposed in Section III with a fixed preview length $L_p = 1.5\text{m}$ and a road profile resolution $\Delta l = 1\text{cm}$.

FTP-MPC: A traditional preview MPC controller with a fixed preview time $t_p = 5T_s$. For different vehicle speeds, the preview data is obtained according to (9) and (10) with that $N_{tp} = 5$. The spatial preview lengths of FTP-MPC and Hybrid HV-MPC methods at different speeds are depicted in Fig. 9 where we can see that the preview length of FTP-MPC is highly dependent on the speed.

NP-MPC: A non-preview controller degraded from the FTP-MPC method with all the preview data equal to zero. This is actually the constrained controller given in [41] where the road disturbance is always assumed to be a white noise.

Skyhook: A classical semi-active suspension controller with a regulation law as follows:

$$u = \begin{cases} c_{\min}(\dot{z}_s - \dot{z}_u) & \text{if } \dot{z}_s(\dot{z}_s - \dot{z}_u) < 0 \\ c_{\max}(\dot{z}_s - \dot{z}_u) & \text{otherwise} \end{cases} \quad (31)$$

where $c_{\min} = 1000\text{Ns/m}$ and $c_{\max} = \kappa = 7000\text{Ns/m}$ are the approximated minimal and maximal damping coefficients that the MR damper can realize.

Soft and Hard: Passive suspensions where the damping coefficient is always equal to c_{\min} for the soft type or c_{\max} for the hard type.

In the following, these control methods will be respectively evaluated under two typical pavements named: independent long-wave roads and serial short-wave roads.

1) *Independent long-wave roads:* A independent bump shown in Fig. 10 is used here to simulate long-wave pavement. Given the bump length and height, the pavement can be described by a sinusoidal function as given in [21].

Firstly, we set the height and length of the bump to 5cm and 1m respectively. By driving through the bump at different speeds, we can get the suspension responses controlled by different algorithms. Fig. 11 shows the response peak-to-peak (PP) value and root-mean-square (RMS) value of signal \ddot{z}_s when the vehicle speed ranges from 3m/s to 25m/s. Further, Fig. 12 shows the time response curves at three typical speeds (4m/s for low speed, 15m/s for medium speed and 22m/s for high speed). Also, Fig. 12 shows the damping force at

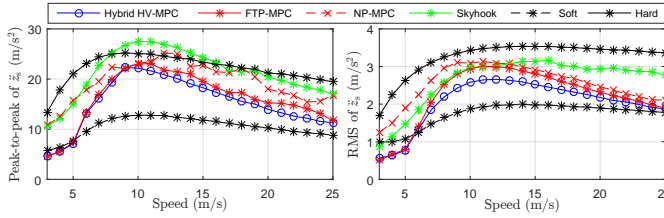


Fig. 11. PP and RMS results under a bump with 1m wavelength.

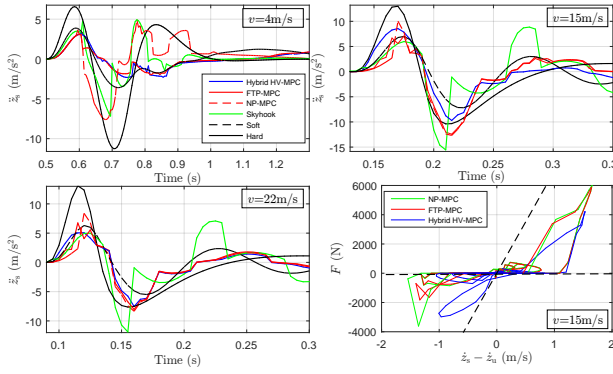


Fig. 12. Responses at different speeds in time domain and the output damping force.

15m/s as an example, where we can see that the nonlinear constraint can be satisfied for all MPC controllers, and the same situation can be found at other speeds. According to Fig. 11, the preview controllers (hybrid HV-MPC and FTP-MPC) are significantly better than the non-preview controllers (NP-MPC and Skyhook) at all speeds. Further, comparing the hybrid HV-MPC and FTP-MPC, it can be found that, for low speeds ($v < 5 \text{ m/s}$), the effects of the two methods are almost identical, including the PP values, the RMS values and the time responses in Fig. 12. Considering that the preview length of FTP-MPC is really short at low speeds, we can figure out that even limited future road information is valuable. But is it unnecessary to increase the preview length? A negative answer can be obtained based on the results at medium speed ($5 \text{ m/s} < v < 20 \text{ m/s}$) where we can see that although the PP values resulted from the two preview controllers are similar, hybrid HV-MPC exhibits better RMS values than FTP-MPC. This phenomenon can be explained by the results at 15m/s in Fig. 12 where hybrid HV-MPC has a relatively larger wave peak just after entering the bump, but it can significantly suppress the subsequent wave trough and the oscillation after leaving the bump. This is actually the superiority of a long-term vision. For higher speed condition ($v > 20 \text{ m/s}$), this superiority will vanish due to the increase of FTP-MPC preview length.

Another phenomenon revealed by Fig. 11 is that, for all the control methods, the comfort performance will first deteriorate and then become better as the vehicle speed increases. Further, by increasing the bump length to 3m, we can obtain the response results in Fig. 13. According to Fig. 13, the long-term vision advantage of hybrid HV-MPC over FTP-MPC is not obvious, since both preview controllers cannot cover the entire

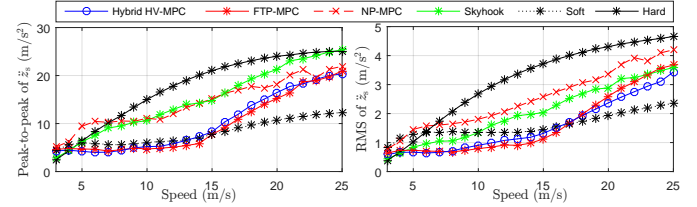


Fig. 13. Peak and RMS results under a bump with 3m wavelength.

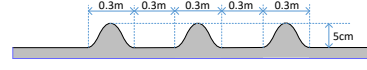


Fig. 14. A pavement with serial short-wave bumps.

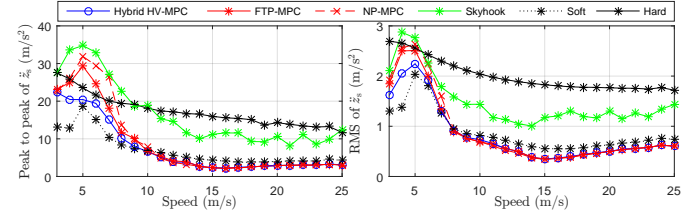


Fig. 15. PP and RMS results under serial short-wave bumps.

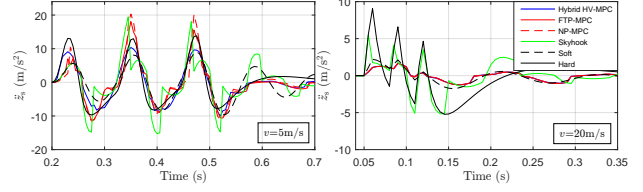


Fig. 16. Time domain responses at different speeds for serial short-wave bumps.

bump. Additionally, unlike Fig. 11, the comfort performance in Fig. 13 always deteriorates as the speed increases. This is understandable, since the results of 3m wavelength are actually those of $v < (25/3) \text{ m/s}$ in Fig. 11 according to the frequency characteristic.

2) *Serial short-wave roads:* In actual driving condition, the bump may not appear independently. For example, in [46] and [47], the pavement geometry with serial bumps has been introduced. Therefore, three serial bumps with a short wavelength shown in Fig. 14 are employed to test the control algorithms. Since every individual bump of this road is same with that in Fig. 10, the serial bumps will show the significance of long length preview for short-wave excitations more clearly. The PP and RMS results at different speeds are given in Fig. 15, while the time-domain responses at two typical speeds (5m/s and 20m/s) are shown in Fig. 16. According to Fig. 15, three MPC methods shows obviously better comfort performance than Skyhook method at all speed conditions. However, there is a certain difference among the three MPC methods with the change of speed. Specifically, at low speed ($v < 8 \text{ m/s}$), FTP-MPC shows better performance than NP-MPC, while hybrid HV-MPC exhibits the best comfort performance. A explanation of this phenomenon can be found according to the responses at 5m/s in Fig. 16, where hybrid HV-MPC

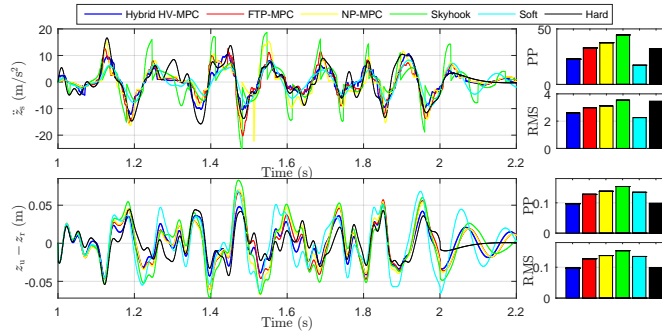


Fig. 17. Responses under a random road profile.

can effectively suppress the vibration caused by the latter two bumps, whereas FTP-MPC only has an effect on the first vibration peak. This actually highlights the significance of long-term vision. Further, at high speed ($v > 8\text{m/s}$), the performance of the three MPC methods is almost identical. Thus, the preview mechanism has no effect in this case. An intuitive understanding comes from the response at 20m/s in Fig. 16, where all of the MPC methods show soft enough characteristics to cope with the high-speed (or high-frequency) disturbance. Another noteworthy thing is that at high speeds, the preview information for such short-wave pavements faces serious distortion problems. For example, the resolution of Θ is that $vT_s = 0.1\text{m}$ which is unable to accurately describe a pavement with 0.3m wavelength. However, due to that preview is ineffective for such condition, the distortion problem does not cause any performance degradation.

Considering that common random roads composed of different harmonics are also a kind of series short-wave road, we further give the response results when the vehicle passes a random road at 5m/s in Fig. 17. Here, the energy distribution of different harmonics satisfies the ISO(International Organization for Standardization) 8608 standard. A detail generation of this random road can be referred in [21]. According to Fig. 17, we can clearly see that hybrid HV-MPC exhibits the minimal \ddot{z}_s than other control methods and can approach the effect of the soft passive suspension. Similar control advantages can also be found in $z_u - z_r$, where the PP and RMS values obtained by hybrid HV-MPC is very close to those of the hard passive suspension. Therefore, hybrid HV-MPC has the ability to simultaneously optimize comfort and handling performance, although only comfort is concerned in this paper.

Additionally, Fig. 15 also indicates that comfort performance will improve as the speed increases, which is completely different from the situation of long-wave roads. Due to the complex road conditions, the relationship between speed and comfort will not always be monotonous, which makes the proposed speed planning method necessary.

B. Multi-Objective Performance at Planned Speed

A road profile shown in Fig. 18 is employed to test the speed planning method and the performance of hybrid HV-MPC at time-varying speeds. The random profiles between bump roads satisfy the ISO 8608 standard. By applying the method given

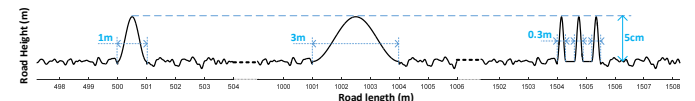


Fig. 18. A driving path consisting of different rough roads and random roads.

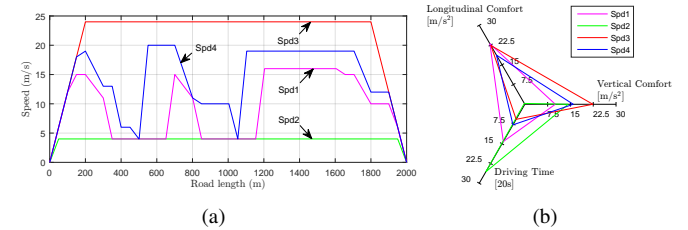


Fig. 19. (a) Speed trajectories; (b) Optimized performance.

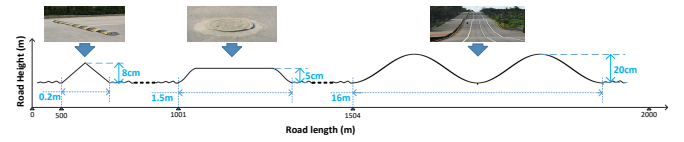


Fig. 20. A typical uneven road profile.

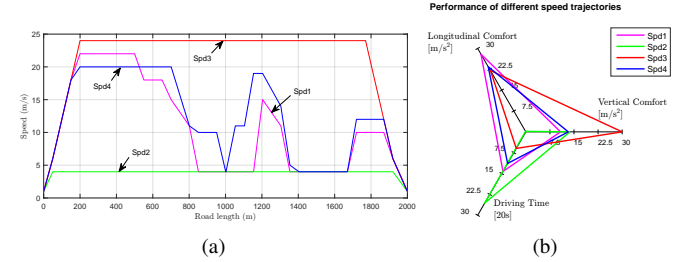


Fig. 21. (a) Speed trajectories; (b) Optimized performance.

in Section IV with $v^{\min} = 4\text{m/s}$ and $v^{\max} = 24\text{m/s}$, different speed trajectories can be obtained in Fig. 19 with the following weighting coefficients:

$Spd1$: $\rho_1 = 50, \rho_2 = \rho_3 = 1$; $Spd2$: $\rho_2 = 50, \rho_1 = \rho_3 = 1$; $Spd3$: $\rho_3 = 50, \rho_1 = \rho_2 = 1$; $Spd4$: $\rho_1 = 6, \rho_2 = 0.5, \rho_3 = 1$. Therefore, $Spd1$, $Spd2$ and $Spd3$ stand for the optimization of vertical comfort, longitudinal comfort and driving time, respectively. By selecting the appropriate weights, $Spd4$ represents the result of multi-objective optimization.

According to Fig. 19(a), it is reasonable that $Spd2$ coincides with v^{\min} such that the sum of longitudinal accelerations can be minimized, and $Spd3$ runs along v^{\max} to minimize travel time. While for the optimal vertical performance, $Spd1$ shows the minimal speed for long-wave bumps and the a high speed for serial short-wave bumps, which is accordance with the patterns indicated by Figs. 11, 13 and 15. Comparing the results of $Spd1$, $Spd2$ and $Spd3$ in Fig. 19(b), it is obvious that there is mutual restriction among the three performance. Therefore, $Spd4$ with multi-objective optimization is preferred. Additionally, comparing $Spd3$ and $Spd4$ in Fig. 19(b), we can see that a significant improvement in vertical comfort performance can be achieved at the expense of very little time consumption. In order to more vividly reflect the above

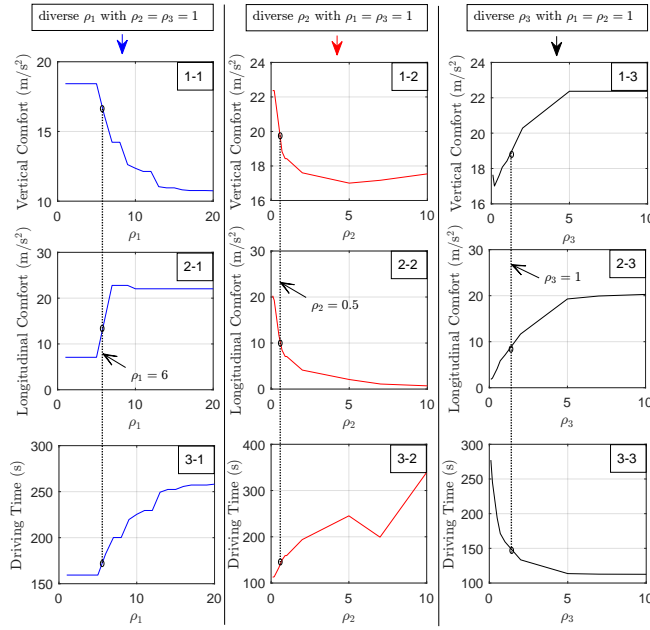


Fig. 22. Multi-objective performance under speed trajectories planned by different weighting parameters.

advantages, Fig. 20 shows a typical driving path composed of several common road incentives (including a speed bump, a manhole cover, a continuous undulating road and random profiles which satisfy the ISO 8608 standard). The speed trajectories planned with different weighting parameters are shown in Fig. 21(a) and the corresponding performance is given in Fig. 21(b). According to Fig. 21, we can also see the superiority of multi-objective planned trajectory *Spd4*.

In order to show in detail the impact of weighting parameters on the speed trajectory and the final performance, Fig. 22 shows the performance of the driving path in Fig. 18 in the following cases:

- 1) $\rho_1 \in [1, 20]$, $\rho_2 = \rho_3 = 1$ (refer to 1-1, 2-1 and 3-1);
 - 2) $\rho_2 \in [0.1, 10]$, $\rho_1 = \rho_3 = 1$ (refer to 1-2, 2-2 and 3-2);
 - 3) $\rho_3 \in [0.1, 10]$, $\rho_1 = \rho_2 = 1$ (refer to 1-3, 2-3 and 3-3).
- According to Fig. 22, we can see that increasing a certain weighting parameter can significantly improve its corresponding performance. Specifical examples are shown in 1-1, 2-2, and 3-3, where increasing ρ_1 , ρ_2 , or ρ_3 can improve vertical comfort, longitudinal comfort, and driving time, respectively. However, the same increasing will lead to the degradation of most other performance. For example, the situations in 2-1, 3-1, 3-2, 1-3, and 2-3. Therefore, in order to achieve multi-objective optimization, this paper selects the circled parameters in Fig. 22 when determining *Spd4*. In practical applications, these parameters can also be set according to user needs.

According to the structure proposed in Fig. 8, we apply the hybrid HV-MPC method with speed adaptability at the different planned speed trajectories in Fig. 19. Fig. 23 shows the responses of \ddot{z}_s when hybrid HV-MPC is combined with *Spd2*, *Spd3* and *Spd4*. From Fig. 23, we can clearly see that driving with *Spd4* can significantly improve the comfort performance at the three rough roads. Additionally, a higher

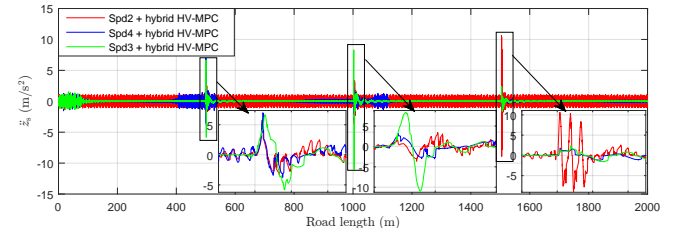


Fig. 23. Responses of hybrid HV-MPC controlled suspension at different speed trajectories.

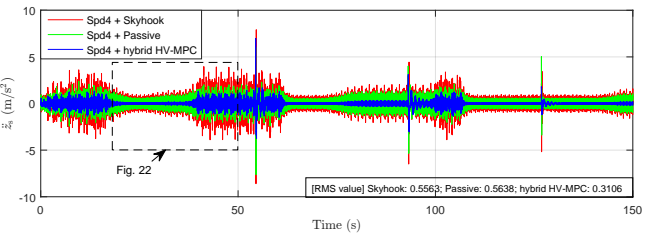


Fig. 24. Responses of different control methods at Spd4 trajectory.

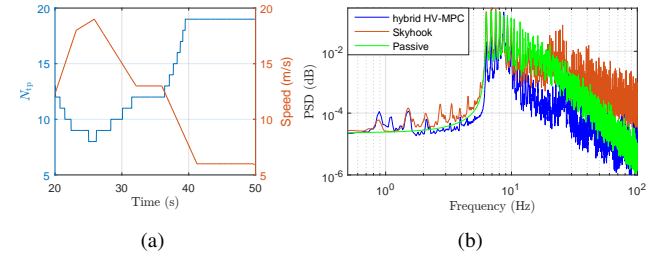


Fig. 25. (a) Variation of speed and prediction horizon; (b) PSD of \ddot{z}_s .

speed can result to better comfort performance at the random roads, which reconfirms the conclusion drawn for the serial short-wave roads. Further, Fig. 24 compares the results of skyhook, passive and hybrid HV-MPC methods when the *Spd4* trajectory is encountered. Here, passive method stands for the suspension which we use in the vertical performance simulator. According to Fig. 24, hybrid HV-MPC delivers the best comfort performance for the same speed variation. Fig. 25 shows the variation of N_{tp} and the PSD results of \ddot{z}_s under a part of random road. From Fig. 25, we can see that the performance advantage of hybrid HV-MPC over other controllers is still evident, even when frequent controller switching occurs.

VI. CONCLUSION

A comfort optimization strategy which can coordinate speed variation and suspension vibration is presented in this paper. Firstly, by combing the given methods of preview information processing and hybrid HV-MPC, the preview semi-active suspension system can fully utilize the road information within the preview range while adapting to speed variation. Secondly, considering the influence of speed on the vibration source, a speed planning problem is constructed in the spatial domain and a dynamic programming solution is given. Finally, the hybrid MPC and speed planning methods are combined and

run in harmony. The simulation results show that, under fixed speeds, the hybrid HV-MPC method can take advantage of the long-term vision and effectively improve the comfort performance. Additionally, it is also indicated that, for different uneven roads, the speed has different impact on the comfort performance. Furthermore, simulations under multiple uneven roads verify that the speed planning method can realize the multi-objective optimization, including vertical vibration, driving time and speed variation. Driving the hybrid HV-MPC controlled suspension under the planned speed also indicates the significance of vertical and longitudinal coordination.

REFERENCES

- [1] R. Bishop, "Intelligent vehicle applications worldwide," *IEEE Intell. Syst.*, vol. 15, no. 1, pp. 78–81, Jan./Feb. 2000.
- [2] J. Armengol, A. Escalera, C. Hilario *et al.*, "IVVI: Intelligent vehicle based on visual information," *Robot. and Auton. Syst.*, vol. 55, no. 12, pp. 904–916, 2007.
- [3] W. Sun, J. Zhang, and Z. Liu, "Two-time-scale redesign for antilock braking systems of ground vehicles," *IEEE Trans. Ind. Electron.*, vol. 66, no. 6, pp. 4577–4586, Jun. 2019.
- [4] H. Kuang, L. Chen, L. Chan, R. Cheung, and H. Yan, "Feature selection based on tensor decomposition and object proposal for night-time multiclass vehicle detection," *IEEE Trans. Syst., Man, Cybern., Syst.*, vol. 49, no. 1, pp. 71–80, Jan. 2019.
- [5] L. Du, Z. Wang, L. Wang, Z. Zhao, F. Su, B. Zhuang, and N. V. Boulgouris, "Adaptive visual interaction based multi-target future state prediction for autonomous driving vehicles," *IEEE Trans. Veh. Technol.*, vol. 68, no. 5, pp. 4249–4261, 2019.
- [6] H. Guo, C. Shen, H. Zhang, H. Chen, and R. Jia, "Simultaneous trajectory planning and tracking using an mpc method for cyber-physical systems: A case study of obstacle avoidance for an intelligent vehicle," *IEEE Trans. Ind. Informat.*, vol. 14, no. 9, pp. 4273–4283, Sep. 2018.
- [7] Y. Wang, Z. Liu, Z. Zuo, Z. Li, L. Wang, and X. Luo, "Trajectory planning and safety assessment of autonomous vehicles based on motion prediction and model predictive control," *IEEE Trans. Veh. Technol.*, vol. 68, no. 9, pp. 8546–8556, 2019.
- [8] G. Quaglia and M. Sorli, "Air suspension dimensionless analysis and design procedure," *Vehicle Syst. Dyn.*, vol. 35, no. 6, pp. 443–475, 2001.
- [9] Y. Liu, Q. Zeng, L. Liu, and S. Tong, "An adaptive neural network controller for active suspension systems with hydraulic actuator," *IEEE Trans. Syst., Man, Cybern., Syst.*, vol. PP, pp. 1–10, Oct. 2018.
- [10] S. Yan and W. Sun, "Self-powered suspension criterion and energy regeneration implementation scheme of motor-driven active suspension," *Mech. Syst. and Signal Pr.*, vol. 94, pp. 297–311, 2017.
- [11] J. Wu, H. Zhou, Z. Liu, and Q. Gu, "A load-dependent PWA- H_∞ controller for semi-active suspensions to exploit the performance of MR dampers," *Mech. Syst. and Signal Pr.*, vol. 127, pp. 441–462, 2019.
- [12] M. Morato, O. Sename, L. Dugard, and M. Nguyen, "Fault estimation for automotive electro-rheological dampers: LPV-based observer approach," *Control Eng. Pract.*, vol. 85, pp. 11–22, 2019.
- [13] S. Savaresi and C. Spelta, "Mixed sky-hook and ADD: Approaching the filtering limits of a semiactive suspension," *J. Dyn. Syst. - T. ASME*, vol. 129, no. 4, pp. 382–392, 2007.
- [14] L. Viet, N. Nghia, N. Hieu *et al.*, "On a combination of ground-hook controllers for semi-active tuned mass dampers," *J. Mech. Sci. and Technol.*, vol. 28, no. 6, pp. 2059–2064, 2014.
- [15] L. Zong, X. Gong, C. Guo, and S. Xuan, "Inverse neuro-fuzzy MR damper model and its application in vibration control of vehicle suspension system," *Vehicle Syst. Dyn.*, vol. 50, no. 7, pp. 1025–1041, 2012.
- [16] H. Du, K. Sze, and J. Lam, "Semi-active H_∞ control of vehicle suspension with magneto-rheological dampers," *J. Sound Vib.*, vol. 283, no. 3–5, pp. 981–996, 2005.
- [17] N. Giorgetti, A. Bemporad, H. Tseng, and D. Hrovat, "Hybrid model predictive control application towards optimal semi-active suspension," *Int. J. Control.*, vol. 79, no. 5, pp. 521–533, 2006.
- [18] M. Canale, M. Milanese, and C. Novara, "Semi-active suspension control using "fast" model-predictive techniques," *IEEE Trans. Control Syst. Technol.*, vol. 14, no. 6, pp. 1034–1046, Nov. 2006.
- [19] L. Cséko, M. Kvasnica, and B. Lantos, "Explicit MPC-based RBF neural network controller design with discrete-time actual kalman filter for semiactive suspension," *IEEE Trans. Control Syst. Technol.*, vol. 23, no. 5, pp. 1736–1753, Sep. 2015.
- [20] C. Poussot-Vassal, O. Sename, L. Dugard *et al.*, "A new semi-active suspension control strategy through LPV technique," *Control Eng. Pract.*, vol. 16, pp. 1519–1534, 2008.
- [21] J. Wu, Z. Liu, and W. Chen, "Design of a piecewise affine H_∞ controller for MR semiactive suspensions with nonlinear constraints," *IEEE Trans. Control Syst. Technol.*, vol. 27, no. 4, pp. 1762–1771, May 2019.
- [22] M. V. D. Aa, J. Muijderman, and F. Veldpaus, "Constrained optimal control of semi-active suspension systems with preview," *Vehicle Syst. Dyn.*, vol. 28, no. 4–5, pp. 307–323, 1997.
- [23] T. Gordon and R. Sharp, "On improving the performance of automotive semi-active suspension systems through road preview," *J. Sound Vib.*, vol. 217, no. 1, pp. 163–180, 1998.
- [24] R. Prabakar, C. Sujatha, and S. Narayanan, "Optimal semi-active preview control response of a half car vehicle model with magnetorheological damper," *J. Sound Vib.*, vol. 326, no. 3–5, pp. 400–420, 2009.
- [25] C. Görhrle, A. Schindler, A. Wagner, and O. Sawodny, "Model predictive control of semi-active and active suspension systems with available road preview," in *European Control Conference (ECC)*, Zurich, Switzerland, Dec. 2013, pp. 1499–1504.
- [26] K. Çalışkan, R. Henze, and F. Küçükay, "Potential of road preview for suspension control under transient road inputs," *IFAC-PapersOnLine*, vol. 49, no. 3, pp. 117–122, 2016.
- [27] P. Li, J. Lam, and K. Cheung, "Velocity-dependent multi-objective control of vehicle suspension with preview measurements," *Mechatronics*, vol. 24, no. 5, pp. 464–475, 2014.
- [28] Y. Qin, Z. Wang, C. Xiang, E. Hashemi, A. Khajepour, and Y. Huang, "Speed independent road classification based on vehicle response: Simulation and experiment," *Mech. Syst. and Signal Pr.*, vol. 117, pp. 653–666, 2019.
- [29] Z. Li, I. Kolmanovsky, E. Atkins *et al.*, "Road risk modeling and cloud-aided safety-based route planning," *IEEE T. Cybernetics*, vol. 46, no. 10, pp. 2473–2483, Nov. 2015.
- [30] ———, "Road disturbance estimation and cloud-aided comfort-based route planning," *IEEE T. Cybernetics*, vol. 47, no. 11, pp. 3879–3891, Nov. 2017.
- [31] M. Lathkar, P. Shendge, and S. Phadke, "Active control of uncertain seat suspension system based on a state and disturbance observer," *IEEE Trans. Syst., Man, Cybern., Syst.*, vol. PP, pp. 1–11, 2017.
- [32] C. Görhrle, A. Schindler, A. Wagner, and O. Sawodny, "Road profile estimation and preview control for low-bandwidth active suspension systems," *IEEE/ASME Trans. Mechatronics*, vol. 20, no. 5, pp. 2299–2310, Oct. 2015.
- [33] X. Yin, L. Zhang, Y. Zhu *et al.*, "Robust control of networked systems with variable communication capabilities and application to a semi-active suspension system," *IEEE/ASME Trans. Mechatronics*, vol. 21, no. 4, pp. 2097–2107, Aug. 2016.
- [34] S.-C. Hung, X. Zhang, A. Festag, K.-C. Chen, and G. Fettweis, "Vehicle-centric network association in heterogeneous vehicle-to-vehicle networks," *IEEE Trans. Veh. Technol.*, vol. 68, no. 6, pp. 5981–5996, 2019.
- [35] J. Mei, K. Zheng, L. Zhao, L. Lei, and X. Wang, "Joint radio resource allocation and control for vehicle platooning in LTE-V2V network," *IEEE Trans. Veh. Technol.*, vol. 67, no. 12, pp. 12218–12230, 2018.
- [36] J. Cao, H. Liu, P. Li *et al.*, "State of the art in vehicle active suspension adaptive control systems based on intelligent methodologies," *IEEE Trans. Intell. Transp. Syst.*, vol. 9, no. 3, pp. 392–405, Sep. 2008.
- [37] X. Tang, X. Hu, W. Yang, and H. Yu, "Novel torsional vibration modeling and assessment of a power-split hybrid electric vehicle equipped with a dual-mass flywheel," *IEEE Trans. Veh. Technol.*, vol. 67, no. 3, pp. 1990–2000, 2018.
- [38] T. Liu, X. Tang, H. Wang, H. Yu, and X. Hu, "Adaptive hierarchical energy management design for a plug-in hybrid electric vehicle," *IEEE Trans. Veh. Technol.*, vol. 68, no. 12, pp. 11513–11522, 2019.
- [39] J. C. Dixon, *Suspension geometry and computation*. Wiltshire, United Kingdom: John Wiley and Sons, 2009, ch. 3.
- [40] D. Wang and W. Liao, "Magnetorheological fluid dampers: a review of parametric modelling," *Smart Mater. Struct.*, vol. 20, p. 023001, 2011.
- [41] A. Bemporad and M. Morari, "Control of systems integrating logic, dynamics, and constraints," *Automatica*, vol. 35, no. 3, pp. 407–427, 1999.
- [42] Y. Zheng, S. Li, and X. Wang, "Horizon-varying model predictive control for accelerated and controlled cooling process," *IEEE Trans. Ind. Electron.*, vol. 58, no. 1, pp. 329–336, 2011.
- [43] R. Shekhar and J. Maciejowski, "Robust variable horizon MPC with move blocking," *Syst. Control Lett.*, vol. 61, no. 4, pp. 587–594, 2012.

- [44] S. Lucia, D. Navarro, O. Lucia, P. Zometa, and R. Findeisen, "Optimized FPGA implementation of model predictive control for embedded systems using high-level synthesis tool," *IEEE Trans. Ind. Informat.*, vol. 14, no. 1, pp. 137–145, 2017.
- [45] O. Gurbudak and E. Santi, "FPGA-based model predictive controller for direct matrix converter," *IEEE Trans. Ind. Electron.*, vol. 63, no. 7, pp. 4560–4570, 2016.
- [46] J. C. Dixon, *Suspension geometry and computation*. United Kingdom: John Wiley, 2009.
- [47] A. Kjell and J. Granlund, "Calculation of reference ride quality, using ISO 2631 vibration evaluation," in *36th United Kingdom Group Meeting on Human Response to Vibration*, Farnborough, UK, Sep. 2001, pp. 1–13.



Jian Wu received the B.S. degree in automation and the M.S. degree in the Department of Control Science and Engineering from Harbin Institute of Technology, Harbin, China, in 2012 and 2014, respectively. He is currently working toward Ph.D. degrees in the Department of Control Science and Engineering with Harbin Institute of Technology. His research interests include vehicle dynamics, vibration, and control.



Hongliang Zhou received the M.S. and Ph.D. degrees in Department of Control Science and Engineering from Harbin Institute of Technology, Harbin, China, in 2006 and 2011, respectively.

He was with the Center for Automotive Research of the Ohio State University, Columbus, OH, USA, from 2016 to 2017, as a visiting scholar. He is currently as a lecturer with the Department of Control Science and Engineering, Harbin Institute of Technology. His current research interests include vehicle dynamics, vehicle active safety control system, model predictive control and nonlinear estimation.



Zhiyuan Liu (M'11) received the B.S. degree from the Zhejiang University of Technology, Hangzhou, China, in 1982, and the Ph.D. degree in control science and engineering from the Harbin Institute of Technology, Harbin, China, in 1992. He was a Post-Doctoral Fellow with the Department of Mechanical Engineering, Harbin Institute of Technology, from 1992 to 1994. Since 1994, he has been with the Department of Control Science and Engineering, Harbin Institute of Technology, where he became a Professor in 1999. He is currently a Professor and the Director of the Department of Control Science and Engineering. His current research interests include robotics, robust control, and model predictive control.



Mingqin Gu received the B.S. degree from Henan Polytechnic University, Henan, China in 2006, and Ph.D. degree in Control Science and Engineering from Central South University, Hunan, China in 2013. She is currently an Algorithm engineer in Alibaba-inc Group, Hangzhou, Zhejiang. Her research interests include self-driving car and robotics.